MOLECULAR AND CELLULAR BIOLOGY, Feb. 2008, p. 1136–1146 Vol. 28, No. 3
0270-7306/08/$08.00+0 doi:10.1128/MCB.01566-07


# The Mouse Polyubiquitin Gene *Ubb* Is Essential for Meiotic Progression▽†

Kwon-Yul Ryu,[1] Shamim A. Sinnar,[1] Laura G. Reinholdt,[2] Sergio Vaccari,[3] Susan Hall,[4] Manuel A. Garcia,[5] Tatiana S. Zaitseva,[1] Donna M. Bouley,[5] Kim Boekelheide,[4] Mary Ann Handel,[2] Marco Conti,[3] and Ron R. Kopito[1]*

*Department of Biological Sciences, Bio-X Program, Stanford University, Stanford, California 94305[1]; The Jackson Laboratory, Bar Harbor, Maine 04609[2]; Division of Reproductive Biology, Department of Obstetrics and Gynecology, Stanford University, Stanford, California 94305[3]; Department of Pathology and Laboratory Medicine, Brown University, Providence, Rhode Island 02912[4]; and Department of Comparative Medicine, Stanford University, Stanford, California 94305[5]*

Received 27 August 2007/Returned for modification 5 October 2007/Accepted 12 November 2007

**Ubiquitin is encoded in mice by two polyubiquitin genes, *Ubb* and *Ubc*, that are considered to be stress inducible and two constitutively expressed monoubiquitin (*Uba*) genes. Here we report that targeted disruption of *Ubb* results in male and female infertility due to failure of germ cells to progress through meiosis I and hypogonadism. In the absence of *Ubb*, spermatocytes and oocytes arrest during meiotic prophase, before metaphase of the first meiotic division. Although cellular ubiquitin levels are believed to be maintained by a combination of functional redundancy among the four ubiquitin genes, stress inducibility of the two polyubiquitin genes, and ubiquitin recycling by proteasome-associated isopeptidases, our results indicate that ubiquitin is required for and consumed during meiotic progression. The striking similarity of the meiotic phenotype in $Ubb^{-/-}$ germ cells to the sporulation defect in fission yeast (*Schizosaccharomyces pombe*) lacking a polyubiquitin gene suggests that a meiotic role of the polyubiquitin gene has been conserved throughout eukaryotic evolution.**

Precisely timed destruction of key cell cycle regulators by the ubiquitin (Ub)-proteasome system orchestrates the complex biochemical events that control the eukaryotic cell division cycle, ensuring its fidelity and unidirectionality (26). The central event in this process is the covalent conjugation of Ub, a versatile, small protein that, in addition to its well-established role in directing protein destruction by the proteasome, serves a multitude of signaling functions in all eukaryotic cells, ranging from membrane trafficking to transcriptional regulation (14, 15). This critical dependence on Ub-dependent processes imposes a stringent requirement on cells to maintain adequate supplies of available Ub.

Cellular Ub exists in a dynamic equilibrium between Ub conjugates and free Ub monomer, maintained by the opposing activities of E3 Ub ligases and Ub isopeptidases (9). Ub supplies are ultimately maintained, however, by de novo synthesis of Ub from Ub gene transcripts. In budding yeast (*Saccharomyces cerevisiae*), Ub is encoded by four genes, three of which (*UBI1*, *UBI2*, and *UBI3*) encode fusion proteins between Ub and small protein components of the large and small ribosomal subunits and one of which (*UBI4*) encodes a Ub polyprotein composed of five Ub moieties arranged in a spacerless, tandem, head-to-tail array (23). *UBI1*, *UBI2*, and *UBI3* supply all of the Ub required for vegetative growth and mitotic cell division, but the polyubiquitin gene, *UBI4*, is essential only during stress (12). Mammalian genomes have four functional Ub genes: two Ub-ribosomal fusion genes, *Uba52* (accession no. MGI:98887) and *Uba80* (accession no. MGI:1925544; also known as *Rps27a*); and two polyubiquitin genes, *Ubb* (accession no. MGI:98888) and *Ubc* (accession no. MGI:98889), consisting of four and nine tandem Ub coding units, respectively (2, 3, 11, 16, 25, 32). The relative contribution of each of these Ub genes to basal Ub levels varies widely among different tissues and cell types (29).

To assess the requirement for maintenance of adequate Ub supplies in cellular function and development, we have generated mice harboring a targeted disruption of the polyubiquitin B (*Ubb*) gene. Mice lacking one or both copies of *Ubb* develop normally and are viable at birth, but $Ubb^{-/-}$ mice of both genders are infertile. $Ubb^{-/-}$ germ cells progress to the pachytene stage and form apparently normal synaptonemal complexes in both males and females. $Ubb^{-/-}$ spermatocytes form XY bodies containing ubiquitinated histones but ultimately undergo cell death during pachytene, and males exhibit complete testicular degeneration by 2 years of age. $Ubb^{-/-}$ oocytes exhibit a heteromorphic meiotic arrest but do not proceed beyond metaphase I. These findings underscore a critical role for *Ubb* in germ cell development and meiosis.

## MATERIALS AND METHODS

Details of targeting vector construction and generation of $Ubb^{-/-}$ mice are described in the supplemental material.

**Histology.** Testes were isolated and fixed in 10% neutral buffered formalin and kept at 4°C until embedded in 2-hydroxyethyl methacrylate (Technovit 7100, Kulzer, Germany). Three-micrometer sections were stained with periodic acid Schiff and hematoxylin (PAS/H). Photomicrographs were taken on a Zeiss Axiovert 35 microscope using a SPOT RT camera and software from Diagnostics Instruments.

Ovaries were fixed in Bouin's fixative at room temperature for 4.5 h, dehydrated in ethanol, and placed in *n*-butanol overnight before being embedded in

* Corresponding author. Mailing address: Stanford University, Gilbert Room 304A, Mail Code 5020, Stanford, CA 94305. Phone: (650) 723-7581. Fax: (650) 724-9945. E-mail: kopito@stanford.edu.

† Supplemental material for this article may be found at http://mcb.asm.org/.

▽ Published ahead of print on 10 December 2007.

paraffin. Five-micrometer ovarian sections were prepared using a microtome and stained with hematoxylin and eosin by standard protocols.

**Superovulation.** Four females of each genotype ($Ubb^{+/+}$ and $Ubb^{-/-}$) were superovulated with an intraperitoneal injection of 5 IU pregnant mare serum gonadotropin (PMSG; Sigma) followed 48 h later by 5 IU of human chorionic gonadotropin (Sigma). Mice were euthanized 16 h later by $CO_2$ inhalation, and the oviducts were dissected out and removed. The cumulus-oophorus-complex was removed and dissolved with hyaluronidase to facilitate oocyte counting.

**In vitro oocyte maturation.** Two to four females of each genotype ($Ubb^{+/+}$, $Ubb^{+/-}$, and $Ubb^{-/-}$) were primed with an intraperitoneal injection of 5 IU PMSG (Sigma). Mice were euthanized 44 h later by $CO_2$ inhalation, and antral follicles were punctured with a needle to expel germinal vesicle (GV) oocytes. Progression of meiotic maturation of denuded mouse oocytes was scored by monitoring the breakdown of GV (GVBD) with an inverted microscope (Olympus, Melville, NY) fitted with a Hoffman contrast lens. Oocytes showing clear nuclear membranes (GV) and nucleoli were classified as GV stage, those without a visible nuclear structure (i.e., exhibiting GVBD) were classified as GVBD stage, and those metaphase II arrested with a polar body were classified as MII. Time zero was the time of follicle puncture.

**Immunolabeling. (i) Testes.** Meiotic spreads were prepared from spermatocytes and immunolabeled as previously described (27). The antibodies used were anti-synaptonemal complex protein 1 (SYCP1) rabbit immunoglobulin G (IgG) (ab15090, 1:500; Abcam); anti-synaptonemal complex protein 3 (SYCP3) mouse monoclonal IgG1 (clone Cor 10G11/7; Novus); anti-SYCP3 rabbit IgG (1:250; Abcam); anti-phosphorylated histone H2A.X (γH2AX) rabbit IgG (1:800; Upstate); anti-ubiquityl histone H2A (uH2A) mouse IgM (clone E6C5, 1:500; Upstate); and Alexa Fluor 488- or 594-conjugated anti-rabbit IgG, Alexa Fluor 594-conjugated anti-mouse IgG1, and Alexa Flour 594-conjugated anti-mouse IgM (Molecular Probes). (All Alexa-conjugated secondary antibodies were used at 1:1,000.) Meiotic spreads were stained with 4′,6′-diamidino-2-phenylindole (DAPI), mounted in SlowFade antifade solution (Molecular Probes), and imaged using a Leica DMRXE upright fluorescent microscope, a Micromax cooled charge-coupled device camera, and Metamorph image acquisition software.

**(ii) Fetal ovaries.** Fetal ovaries were collected from 18.5-day-postcoitum (dpc) embryos. From each embryo, one ovary was fixed in 4% paraformaldehyde in phosphate-buffered saline (PBS) for 1 h at room temperature and then washed in PBS overnight at 4°C for subsequent embedding and immunolabeling. The other ovary was used to prepare microspread oocyte nuclei. The ovaries were each placed in one well of a multiwell dish containing hypoextraction buffer (15 mM Tris, 50 mM sucrose, 20 mM citrate, 5 mM EDTA, 0.5 mM dithiothreitol [DTT], 0.09 mg/ml phenylmethylsulfonyl fluoride [PMSF], and 0.5 mg/ml collagenase added just prior to use). After 30 min of incubation at room temperature, each ovary was moved to one 10-μl drop of 0.1 M sucrose on a siliconized glass slide. Each ovary was macerated, an additional 10 μl of 0.1 M sucrose was added, and a suspension was made by gentle pipetting. The 20-μl suspension was then pipetted onto a glass slide coated with freshly prepared 1% paraformaldehyde containing 0.1% Triton X-100 (pH 9.2). The slides were incubated in a humid chamber for 4 h at room temperature, moved to the bench top for brief air drying, and then washed three times for 5 min each in 1:250 Photo-Flo (Kodak, Electron Microscopy Sciences). Slides were air dried and immunolabeled according to standard protocols (27). The antibodies used were anti-SYCP1 rabbit IgG (see above), anti-SYCP3 mouse monoclonal IgG1 (see above), Alexa Fluor 594-conjugated anti-rabbit IgG (1:1,000; Molecular Probes), and Alexa Fluor 488-conjugated anti-mouse IgG1 (1:1,000; Molecular Probes).

Embedded fetal ovaries were serially sectioned (5 μm thick), deparaffinized, and treated twice for 5 min each in 50 mM $NH_4Cl$–PBS. Each section was incubated for 1 h at room temperature in blocking solution (10% normal goat serum, 3% bovine serum albumin [BSA], 0.1% Triton X-100 in PBS). Diluted primary antibody (in blocking solution) was applied to each section and incubated for 2 h at room temperature (or at 4°C overnight). Slides were washed three times for 10 min each in 10% blocking solution (in PBS), and diluted secondary antibody was applied to each section. Slides were incubated at room temperature for 2 h and then washed three times for 10 min each in blocking solution. Slides were then stained with DAPI and mounted in SlowFade antifade solution (Molecular Probes). The antibodies used were anti-germ cell nuclear antigen (GCNA) rat IgM (undiluted) (10) and Alexa Fluor 594-conjugated anti-rat IgM (1:1,000; Molecular Probes). Immunolabeled sections were imaged using a Leica DMRXE upright fluorescent microscope, a Micromax cooled charge-coupled device camera, and Metamorph image acquisition software. Immunolabeled slides were then postfixed in 4% paraformaldehyde for 10 min at room temperature to preserve immunolabeling and washed in PBS, and a terminal deoxynucleotidyltransferase-mediated dUTP nick end labeling (TUNEL) assay was performed according to the manufacturer's (Roche) protocol for in situ cell death detection with fluorescein. TUNEL-labeled sections were imaged a second time as described above.

**(iii) Oocytes.** Oocytes were collected from antral follicles after PMSG priming of wild-type (+/+; $n = 1$), heterozygous (+/−; $n = 3$), and knockout (−/−; $n = 4$) females. Fifteen hours past puncture, oocytes were treated with Tyrode's acid for 2 h at room temperature to remove the zona pellucida. They were fixed in a solution containing 0.1% Triton X-100, 4% paraformaldehyde, and 1 μM Taxol for 30 min at 37°C, washed, and blocked with 2% BSA in PBS overnight at 4°C. Oocytes were placed in anti-α-tubulin monoclonal antibody (DMC1, 1:500; Sigma) overnight at 4°C, washed, and then incubated with Alexa Fluor 488-conjugated anti-mouse IgG (1:1,700; Molecular Probes) and DAPI for 2 h at room temperature. Oocytes were mounted using Vectashield.

**Indirect competitive ELISA.** Tissues were homogenized with Potter-Elvehjem tissue grinder with polytetrafluoroethylene pestle (Thomas Scientific) in hypotonic buffer (10 mM sodium phosphate [pH 7.4] with protease inhibitor cocktail; Roche) with 0.1% digitonin and incubated on ice for 20 to 30 min. Tissue lysates were centrifuged at 13,000 rpm for 10 min at 4°C, and the supernatant was removed to measure protein concentration by bicinchoninic acid protein assay (Pierce). To prepare samples for enzyme-linked immunosorbent assay (ELISA), tissue lysates (24 μg) were treated with 2.4 μg Usp2-cc (catalytic core of ubiquitin-specific protease 2) in the presence of 1.4 mM β-mercaptoethanol and 140 mM NaCl in a 20-μl reaction volume for 30 min at 37°C (4, 8). Usp2-cc-treated tissue lysates were further diluted with 1% BSA–PBS containing 0.1% digitonin, and total Ub levels were measured by ELISA as described previously (28). For oocyte ELISA, oocytes at GV and GVBD stages were counted and collected in 3 μl hypotonic buffer containing 0.1% digitonin during maturation in vitro. Oocytes were lysed by repeated freeze-thaw cycle, treated with Usp2-cc, and subjected to ELISA measurement.

**Quantitative real-time RT-PCR.** Total RNA was isolated from RNA*later*-stabilized tissues using the RNeasy Plus kit (Qiagen). The RNA concentration was determined, and 200 ng of total RNA was subsequently treated with DNase I (Invitrogen) and reverse transcribed using iScript select cDNA synthesis kit (Bio-Rad) with oligo(dT) as a primer. For real-time PCR, 1/20 of cDNA was used as a template. Reverse transcription-PCR (RT-PCR) was accomplished using the iQ SYBR green supermix (Bio-Rad) and iCycler system with iCycler iQ software version 3.1 (Bio-Rad), with the following cycle profile: 95°C for 3 min; 45 cycles of 95°C for 10 s, 60°C for 30 s, 68°C for 30 s; 95°C for 1 min; and 55°C for 1 min followed by 80 cycles of 55°C for 10 s with an increase of 0.5°C per cycle for melt curve analysis. The mRNA expression levels of *Ubc*, *Ubb*, *Uba52*, and *Uba80* were normalized to the level of β-actin or 18S rRNA (5). Primers used for real-time RT-PCR were as follows: Ubc-F (5′-GTTACCACCAAGAAGGTC-3′), Ubc-R (5′-GGGAATGCAAGAACTTTATTC-3′), Ubb-F (5′-TCTGAGG GGTGGCTATTAA-3′), Ubb-R (5′-TGCTTACCATGCAACAAAAC-3′), Uba52-F (5′-GTCAGCTTGCCCAGAAGTAC-3′), Uba52-R (5′-ACTTCTTCT TGCGGCAGTTG-3′), Uba80-F (5′-TGGCAAAATTAGCCGACTTCG-3′), Uba80-R (5′-AACACTTGCCACAGTAATGCC-3′), 18S rRNA-F (5′-CGGCT ACCACATCCAAGGAA-3′), and 18S rRNA-R (5′-GCTGGAATTACCGCG GCT-3′). Control plasmid DNA was generated by subcloning each cDNA fragment into the pCR2.1 vector (Invitrogen), and $10^8$ to $10^3$ copies of plasmid DNA were used as a standard.

**Confocal microscopy.** For direct visualization of green fluorescent protein (GFP) fluorescence in testicular and ovarian sections, tissues were fixed in 4% paraformaldehyde for 2 to 4 h at 4°C, cryoprotected with 30% sucrose, and sectioned with a cryostat. Thaw-mounted sections (5 μm thick) were washed with Tris-buffered saline (TBS) and incubated with TO-PRO-3 iodide (1:1,000; Molecular Probes, excitation/emission $\lambda = 642/661$ nm) in 0.3% Triton X-100–TBS (TBST) for 30 min at room temperature for DNA staining. Sections were washed with TBST followed by TBS only and mounted with ProLong Gold antifade reagent (Molecular Probes). To monitor *Ubb* or *Ubc* transcriptional activity, fluorescence from GFP was directly visualized. Confocal images were collected with Leica TCS SP2 laser-scanning system with sequential image recording. The GFP image was collected using a 488-nm excitation light from an Ar laser with the emission window at 500 to 535 nm, and the TO-PRO-3 iodide image was collected using a 633-nm excitation light from an He-Ne laser with the emission window at 650 to 750 nm.

**Statistical analysis.** A two-tailed unpaired Student's $t$ test was used to compare the data between two groups. $P < 0.05$ was considered to be statistically significant.

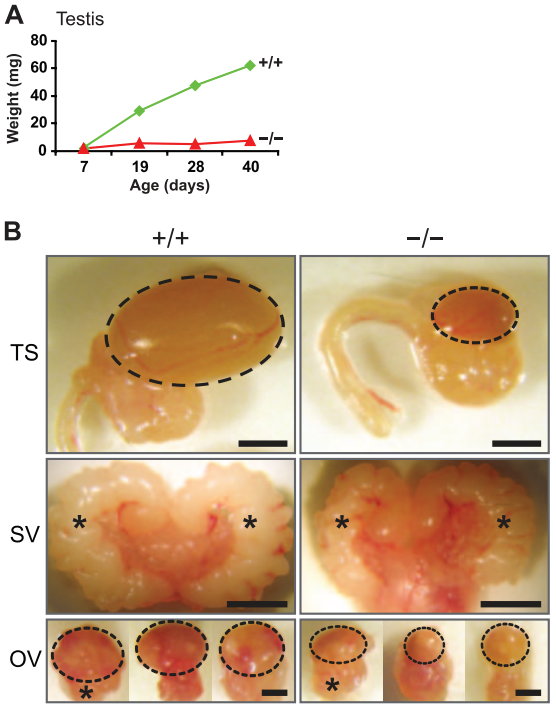


FIG. 1. Gonadal developmental defect of $Ubb^{-/-}$ mice. (A) Testis weights of $Ubb^{+/+}$ and $Ubb^{-/-}$ mice at 7, 19, 28, and 40 days of age. Weights were measured from one testis per animal at each age ($n \geq 2$/age). (B) (Top and middle) Morphology of testes (TS; indicated by black dotted circle) and seminal vesicles (SV; asterisk) in representative 5-month-old $Ubb^{+/+}$ and $Ubb^{-/-}$ mice. (Bottom) Morphology of ovaries (OV; black dotted circle) in 5-month-old $Ubb^{+/+}$ ($n = 3$) and $UbB^{-/-}$ ($n = 3$) mice. Fallopian tubes are indicated by asterisks. Scale bar for TS, 2 mm; scale bar for SV, 5 mm; scale bar for OV, 1 mm.

## RESULTS

***Ubb* gene is required for fertility and postnatal gonadal maturation.** Although testes of 7-day-old $Ubb^{-/-}$ mice were indistinguishable from those of wild-type littermates, they failed to increase in size with age, suggesting that *Ubb* is required for postnatal testicular development (Fig. 1A). At 5 months of age, testes of $Ubb^{-/-}$ mice were substantially smaller, although seminal vesicle weights were very similar to those of littermate controls ($Ubb^{+/+}$ and $Ubb^{+/-}$), suggesting normal Leydig cell function (Fig. 1B; also see Fig. S2 in the supplemental material). Testosterone levels in 5-month-old male mice were not significantly different among different genotypes, supporting the conclusion that Leydig cell function is intact in $Ubb^{-/-}$ mice (data not shown). Ovarian size and weight were also reduced significantly in 5-month-old $Ubb^{-/-}$ females compared to littermate controls (Fig. 1B; also see Fig. S2 in the supplemental material). Interbreeding of homozygous ($Ubb^{-/-}$) males and females did not yield any progeny, although vaginal plugs were observed ($n = 2$). Mating of homozygous males with heterozygous females ($n = 14$) or heterozygous males with homozygous females ($n = 12$) also did not yield any progeny over a 4-month period despite observation of vaginal plugs. These results demonstrate a strict requirement of *Ubb* for male and female fertility in the mouse.

**Spermatogenesis in male $Ubb^{-/-}$ mice is arrested in prophase of meiosis I.** At 7 days of age (d7), $Ubb^{-/-}$ testes display normal histology (Fig. 2A, d7). Seminiferous tubules containing numerous Sertoli cells with radially oriented nuclei are interspersed among abundant spermatogonia. By 19 days, however, marked differences are seen between $Ubb^{+/+}$ and $Ubb^{-/-}$ testes. $Ubb^{+/+}$ testes contain seminiferous tubules with multiple layers of germ cells at different stages of maturation, including those that have completed meiosis to become round spermatids (Fig. 2A, d19, +/+). Some seminiferous tubules have formed lumens, and all Sertoli cells have their nuclei located adjacent to the basement membrane. In contrast, seminiferous tubules from $Ubb^{-/-}$ testes are smaller and contain variable numbers of germ cells (Fig. 2A, d19, −/−). Some of the seminiferous tubules contain abundant Sertoli cells but few spermatogonia (tubule 1), while others contain numerous germ cells that have not matured beyond the early pachytene spermatocyte stage of meiosis I (tubule 2). Furthermore, $Ubb^{-/-}$ testes at 19 days contain large clusters of heteropyknotic germ cells possibly undergoing cell death. Finally, many Sertoli cell nuclei are abnormally separated from the basement membrane and no seminiferous tubule lumens have formed. By 28 days, $Ubb^{+/+}$ testes contain the full complement of germ cell types with multiple generations of germ cells present, whereas the most advanced germ cells in $Ubb^{-/-}$ testes remain in pachytene or are undergoing cell death (data not shown). By 40 days, the first wave of spermatogenesis is complete in $Ubb^{+/+}$ testes; elongated and condensed spermatids are clearly visible (Fig. 2A, d40, +/+). Seminiferous tubule lumens are well formed, and Sertoli cell nuclei are adjacent to the basement membrane. In contrast, $Ubb^{-/-}$ testes contain a paucity of germ cells; these have not matured beyond the pachytene stage (Fig. 2A, d40, −/−). Many of these pachytene spermatocytes are undergoing cell death, as indicated by nuclear condensation and fragmentation. In addition, the testis architecture is severely disrupted, with absent seminiferous tubule lumens, focal clusters of detached Sertoli cells, and prominent interstitial Leydig cells. The last feature could be the result of Leydig cell hyperplasia but most likely reflects the failure of normal seminiferous epithelium growth, resulting in reduced size and mass of the seminiferous tubules. Finally, at 8.5 months, $Ubb^{-/-}$ testes are severely atrophic and completely abnormal; no germ cells are present, and the testes contain only sparse and degenerating Sertoli cells and prominent masses of Leydig cells (data not shown). At 2 years of age, the testes could not be identified due to complete organ degeneration (data not shown). This severe degenerative phenotype, which is not typical of other meiotic arrest mutants, suggests defects beyond those of the germ cells. Thus, germ cells from $Ubb^{-/-}$ mice fail to progress beyond the early pachytene spermatocyte stage of meiosis and undergo cell death; additionally testis development is impaired, with ultimate degeneration.

To further characterize the pachytene arrest, meiotic spreads were prepared from the spermatocytes of 21-day-old $Ubb^{-/-}$ and littermate control ($Ubb^{+/-}$) mice. Immunolabeling with antibodies to the synaptonemal complex proteins SYCP1 and SYCP3 demonstrate that synaptonemal complexes form normally along homologous chromosomes in $Ubb^{-/-}$ pachytene spermatocytes (Fig. 2B). Consistent with the histology data, diplotene nuclei could not be identified in meiotic

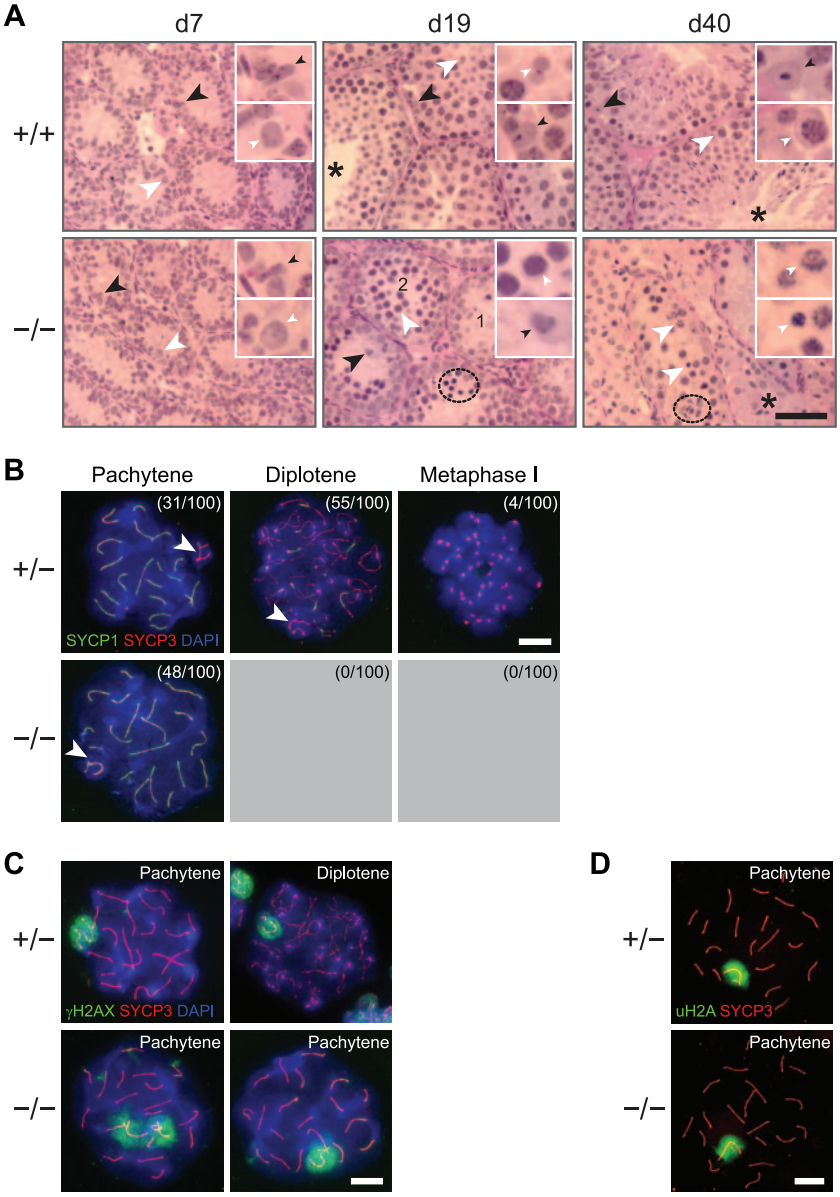


FIG. 2. Impaired meiotic progression in *Ubb*$^{-/-}$ mouse testes. (A) Testis sections from *Ubb*$^{+/+}$ and *Ubb*$^{-/-}$ mice were stained with PAS/H. For both *Ubb*$^{+/+}$ and *Ubb*$^{-/-}$ mice at 7 days (d7), black arrowheads indicate Sertoli cell nuclei and white arrowheads indicate spermatogonia. For *Ubb*$^{+/+}$ mice at 19 days (d19), white arrowheads indicate round spermatids, black arrowheads indicate Sertoli cell nuclei, and an asterisk indicates lumens. For *Ubb*$^{-/-}$ mice at d19, white arrowheads indicate spermatocytes arrested at pachytene stage, black arrowheads indicate Sertoli cell nuclei separated from the basement membrane, and a black dotted circle indicates clusters of germ cells undergoing cell death. For *Ubb*$^{+/+}$ mice at 40 days (d40), black arrowheads indicate Sertoli cell nuclei, white arrowheads indicate spermatocytes, and an asterisk indicates lumens. For *Ubb*$^{-/-}$ mice at d40, white arrowheads indicate pachytene spermatocytes undergoing cell death, an asterisk indicates interstitial Leydig cells, and a black dotted circle indicates clusters of Sertoli cells separated from the basement membrane. The cells indicated by arrowheads were magnified ×3 from the original images and are shown as insets. Scale bar, 50 μm. (B) *Ubb*$^{-/-}$ spermatocytes arrest in pachytene. Meiotic spreads were immunolabeled with anti-SYCP1 (green) and anti-SYCP3 (red) antibodies and DAPI (blue). The developmental stages in meiotic prophase were determined by SYCP3 kinetics, and the numbers of spermatocytes in each stage are indicated. White arrowhead, XY body. Scale bar, 5 μm. (C) Formation of XY body is delayed in *Ubb*$^{-/-}$ mice. Meiotic spreads were immunolabeled with anti-γH2AX (green) and anti-SYCP3 (red) antibodies and DAPI (blue). Scale bar, 5 μm. (D) uH2A is present in XY body of pachytene spermatocytes from *Ubb*$^{-/-}$ mice. Meiotic spreads were immunolabeled with anti-uH2A (green) and anti-SYCP3 (red) antibodies. Scale bar, 5 μm.

spread preparations from *Ubb*$^{-/-}$ spermatocytes, whereas roughly half of *Ubb*$^{+/-}$ spermatocytes were found to be in diplotene at 21 days. The XY body, comprised of the partially synapsed and largely nonhomologous X and Y chromosomes, also forms in *Ubb*$^{-/-}$ pachytene spermatocytes, as indicated by immunolabeling with an antibody against phosphorylated histone H2A.X (γH2AX) (Fig. 2C). This histone modification is associated with the transcriptionally silenced XY body and is normally a discrete focus in the mid-pachytene spermatocytes. In *Ubb*$^{-/-}$ spermatocytes, however, the γH2AX antibody does

not label a discrete XY body in all pachytene spermatocytes (Fig. 2C). This could reflect a delay in the progression of pachynema in $Ubb^{-/-}$ spermatocytes or a delay in the formation of the XY body. Although Ub content is decreased in $Ubb^{-/-}$ testes (see below), the XY body becomes associated with ubiquitinated H2A (uH2A) (Fig. 2D), a modification which is thought to maintain silencing of unpaired chromosomal regions (1). Thus, data from both histology and meiotic chromatin analysis demonstrate a spermatogenetic arrest during pachytene and indicate that *Ubb* is required, either directly or indirectly, for exit from prophase of meiosis I.

**Defective ovarian follicular development and meiotic arrest in female *Ubb*$^{-/-}$ mice.** At 2 and 5 months of age, both $Ubb^{+/+}$ and $Ubb^{+/-}$ females display normal ovarian architecture, with numerous follicles present in different stages of development (primary, secondary, and antral or Graafian follicles), as well as prominent corpora lutea indicative of recent ovulation (Fig. 3A, +/+, and data not shown for $Ubb^{+/-}$). In contrast, ovaries from $Ubb^{-/-}$ females are much smaller (see Fig. 1B) and have few mature follicles and few corpora lutea (Fig. 3A, −/−). Five-month-old $Ubb^{-/-}$ ovaries weigh on average 2 to 3 times less than $Ubb^{+/+}$ and $Ubb^{+/-}$ ovaries (see Fig. S2 in the supplemental material). Because $Ubb^{-/-}$ spermatocytes fail to progress to diplonema, meiotic spread preparations were made from fetal $Ubb^{-/-}$ ovaries to assess whether knockout oocytes could progress to diplonema. Immunolabeling with antibodies against SYCP1 and SYCP3 revealed that, as in spermatocytes, synaptonemal complex proteins assemble normally along synapsed homologous chromosomes during female meiosis. In addition, while some normal diplotene oocyte nuclei were observed, there were also some abnormal diplotene-like nuclei with fragmented and elongated synaptonemal complexes (Fig. 3B). Immunolabeling with an antibody against GCNA and the TUNEL assay revealed that $Ubb^{-/-}$ fetal ovaries have fewer oocytes and elevated apoptotic nuclei (Fig. 3C). Therefore, some $Ubb^{-/-}$ oocytes do not progress normally to diplonema and are likely lost via apoptosis during fetal development. The reduction in ovary size and follicle number in adult $Ubb^{-/-}$ females is likely the result of oocyte loss during fetal development. Despite these abnormalities, the surviving oocytes in immature follicles from adult ovaries appear histologically to be in the normal dictyate (resting) stage of meiosis I. (Mammalian oocytes are arrested in embryonic or early postnatal life after completing the diplotene stage of meiosis I [7, 24] and resume meiosis only at the antral follicle stage [31].)

Following treatment with PMSG, $Ubb^{-/-}$ females formed morphologically normal antral follicles in which oocytes contained a normal-appearing GV (Fig. 3D); however, the size of these antral follicles was smaller than those of $Ubb^{+/+}$ females and never reached more than 100 to 150 μm (data not shown). To determine whether $Ubb^{-/-}$ females are capable of ovulation, they were superovulated with exogenous sources of follicle-stimulating hormone and luteinizing hormone (Fig. 3E). Only rarely did $Ubb^{-/-}$ females ovulate any oocytes, and even these tended to have an abnormal morphology with a thin zona pellucida tightly adherent to the plasma membrane and no evidence of polar bodies (data not shown). These data suggest that *Ubb* is required for meiotic maturation.

To address the nature of the meiotic maturation defect, we assessed the ability of $Ubb^{-/-}$ oocytes to undergo spontaneous maturation in vitro. Whereas over 90% of $Ubb^{+/+}$ (data not shown) and $Ubb^{+/-}$ oocytes underwent nuclear envelope dissolution (GVBD) within 90 min after isolation, GVBD was markedly delayed and ultimately observed in fewer than 70% of $Ubb^{-/-}$ oocytes (Fig. 4A, left). Strikingly, while nearly 80% of $Ubb^{+/+}$ (data not shown) and $Ubb^{+/-}$ oocytes extruded polar bodies after 24 h in vitro, signifying completion of meiosis I, $Ubb^{-/-}$ oocytes were never observed to complete this step (Fig. 4A, right). These results suggest that two sequential defects occur in adult $Ubb^{-/-}$ oocytes. First, many of these oocytes cannot exit meiotic prophase since they cannot undergo GVBD, which occurs at the prophase-to-metaphase transition. Second, those that do exit prophase cannot complete meiosis I and form the first polar body. Oocytes from $Ubb^{+/-}$ females aligned their chromosomes on a well-formed spindle (Fig. 4B, +/−) and also displayed chromosomes and spindle remnants in the polar body. In contrast, chromosomes from $Ubb^{-/-}$ oocytes only rarely aligned on a normal-looking spindle (2/19 oocytes; 10.5%); often, the spindle was malformed (7/19 oocytes; 36.8%) or was not present at all (10/19 oocytes; 52.6%) (Fig. 4B, −/−). Thus, $Ubb^{-/-}$ oocytes cannot successfully negotiate the prophase-to-metaphase transition. The polyubiquitin gene *Ubb* therefore is necessary for proper progression through and exit from meiotic prophase, as well as for pre- and postnatal oocyte development.

**Dominant role of the *Ubb* gene in maintenance of germ cell Ub levels.** The dramatic meiotic phenotypes of male and female $Ubb^{-/-}$ mice suggest that the *Ubb* gene contributes a specific, nonredundant role in Ub homeostasis during germ cell development. To assess the contribution of *Ubb* to the maintenance of Ub pools, we used indirect competitive ELISA (28) to measure total Ub abundance in various organs of 5-month-old mice of different *Ubb* genotypes (Fig. 5A). Of the tissues examined, the Ub concentration (as a fraction of total protein) was highest in testes—nearly double that of brain, the tissue with the next highest Ub concentration—and more than 4 times higher than spleen. The Ub concentration in testes was reduced by homozygous loss of *Ubb* by ~70% (Fig. 5A) in 5-month-old mice and by ~50% (data not shown) in 1-month-old mice. In contrast, Ub levels were largely unaffected by homozygous loss of *Ubb* in all other organs examined. Furthermore, *Ubb* mRNA is the most abundant Ub transcript in testes, constituting ~60% of the total Ub transcripts and ~75% of the total Ub coding "potential" (i.e., when normalized for the number of Ub coding units per transcript) (Fig. 5B and +/+ in Fig. 5C, right). Considering that germ cells comprise ~90% of the cells in the adult testes (20) and that postnatal spermatogenesis is accompanied by an approximate doubling of testicular Ub levels (data not shown), it is probable that the uniquely high levels of Ub in testes are due to the contribution of *Ubb* expression in germ cells.

In contrast, Ub levels in the ovary are comparable to those in other tissues and reduced only ~35% ($P = 0.055$) by homozygous disruption of *Ubb* (Fig. 5A), consistent with the observation that *Ubb* mRNA represents only ~20% of the total Ub transcript in this organ (Fig. 5B) and is predicted to contribute only ~30% of the total Ub coding potential (Fig. 5D, right). We propose that the dramatic phenotype observed in $Ubb^{-/-}$ ovaries, despite the relatively minor contribution of *Ubb* to total Ub pools in this tissue, reflects the fact that oocytes constitute only a small fraction

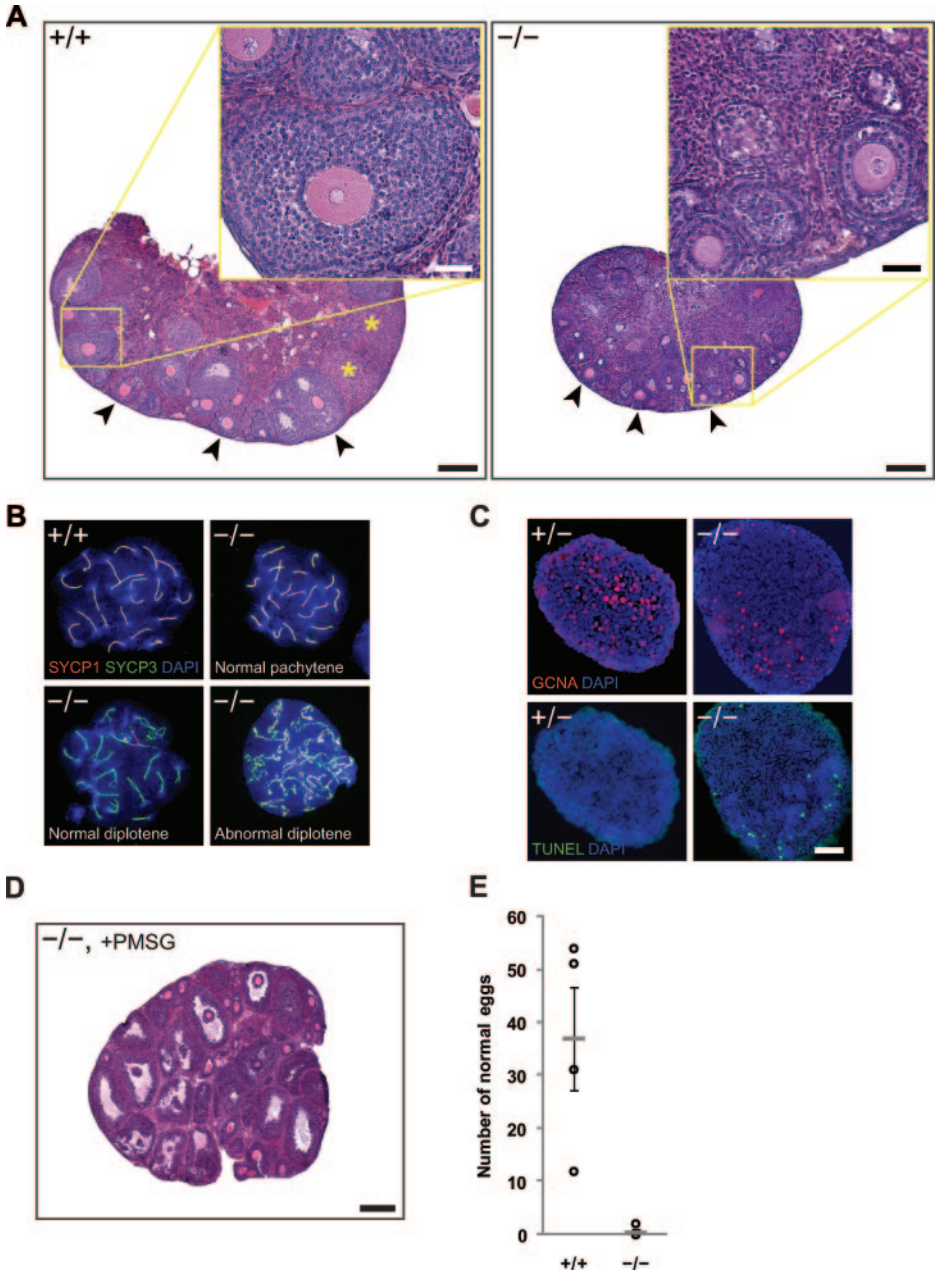


FIG. 3. Defective ovarian development and meiotic progression in $Ubb^{-/-}$ mice and embryos. (A) Histology of ovaries from $Ubb^{+/+}$ and $Ubb^{-/-}$ females. Follicles and corpora lutea are indicated by black arrowheads and asterisks, respectively. Scale bar, 500 μm; inset, 200 μm. (B) Heteromorphic arrest of meiosis in $Ubb^{-/-}$ oocytes. Meiotic spreads were prepared from $Ubb^{+/+}$ and $Ubb^{-/-}$ embryonic day 18.5 (E18.5) embryos and immunolabeled with anti-SYCP1 (red) and anti-SYCP3 (green) antibodies and DAPI (blue). (C) Increased apoptosis in $Ubb^{-/-}$ oocytes. Ovarian sections were prepared from E18.5 embryos and immunolabeled with anti-GCNA antibody (top) or assayed for TUNEL-positive nuclei (bottom). DNA was stained with DAPI. Scale bar, 100 μm. (D) Histology of ovary following superovulation. Scale bar, 500 μm. (E) Impaired ovulation in $Ubb^{-/-}$ mice. Oocytes were counted in dissected oviducts from superovulated mice ($n$ = 4/genotype). Bars denote the mean ± standard error for each condition.

of the mass of this tissue. In fact, the Ub concentration in isolated GV oocytes from wild-type mice is 0.24 ± 0.01 ng/oocyte (Fig. 5E), corresponding to approximately 10 μg/mg protein (19), and is directly comparable to the level in whole testes. Total Ub levels in freshly isolated GV oocytes from $Ubb^{-/-}$ mice were about 70% lower than in the wild type, confirming the overwhelming contribution of *Ubb* to maintenance of oocyte Ub levels (Fig. 5E). Moreover, Ub levels fell significantly—by nearly 25%—upon GVBD in wild-type oocytes, suggesting that Ub is consumed during meiotic prophase. These data unequivocally establish that *Ubb* is the principal source of Ub in oocytes and that, in its absence, Ub levels decline during prophase I to less than 25% of wild-type levels, even in the absence of such dramatic Ub deficiency in whole ovary.

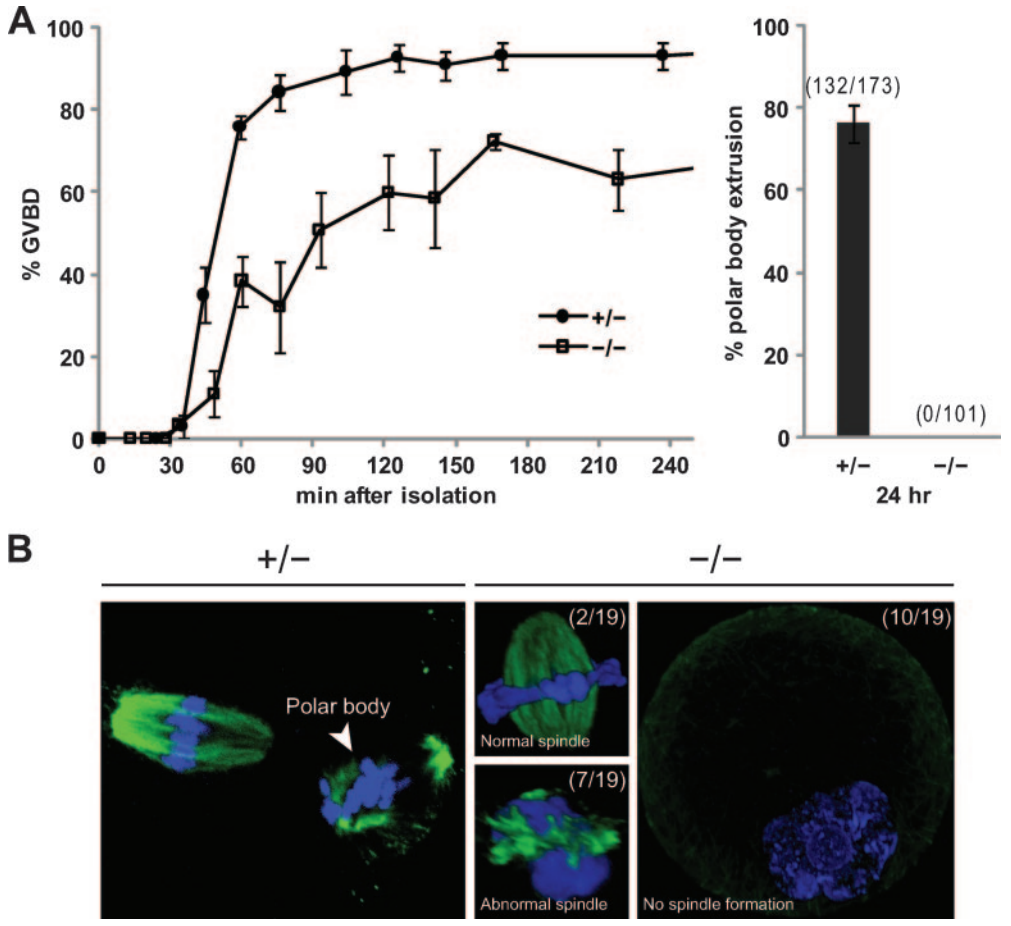


FIG. 4. Impaired meiotic progression in $Ubb^{-/-}$ mouse oocytes in vitro. (A) Delayed and impaired GVBD (left) and absent polar body extrusion (right) in oocytes isolated from $Ubb^{-/-}$ mice and allowed to undergo spontaneous maturation in vitro ($n = 3$ to 4/genotype). (B) Spindle morphologies of in vitro-matured oocytes. Oocytes were labeled with antibody to α-tubulin (green) and with DAPI (blue). Out of 19 oocytes examined, 2 formed a normal-appearing spindle, 7 formed aberrant spindles, and 10 failed to form any spindle.

Although *Ubc*, like *Ubb*, is known to be stress inducible and contains heat shock elements (6, 13, 29), changes in *Ubc* transcript levels in $Ubb^{-/-}$ testes (Fig. 5C) and ovaries (Fig. 5D) are insufficient to compensate for the reduced Ub levels resulting from the loss of *Ubb*, even after correcting for the greater number of Ub coding units in *Ubc* mRNA. Surprisingly, we observed substantially increased levels of *Uba* transcripts in both testes and ovaries of $Ubb^{-/-}$ mice (Fig. 5C and D), reflecting a limited capacity of *Uba* genes to respond to Ub deficiency or perhaps an increased relative mass of cells in which the *Uba* genes contribute a higher proportion of total Ub.

**Complementary patterns of polyubiquitin gene expression in gonads.** In order to understand the consequences of loss of the *Ubb* and *Ubc* genes on Ub levels and germ cell maturation, it is necessary to identify the cell types in which these two genes are normally expressed. However, because the final protein products of all four Ub genes are chemically identical, it is not feasible to use immunohistochemistry to assess the spatial expression of these genes. We therefore, took advantage of the GFP-puro cassette that precisely replaces the polyubiquitin coding exons in the target construct to monitor polyubiquitin gene promoter activity (29). Since the promoter and all other regulatory elements of the *Ubb* and *Ubc* genes remain intact following recombinatorial disruption of the coding exon, the spatial expression of *Ubb* and *Ubc* genes can be assessed by GFP expression analysis (Fig. 6). Control experiments confirmed that the relative levels of GFP mRNA in tissues from $Ubb^{+/-}$ and $Ubc^{+/-}$ mice were correlated with the levels of *Ubb* and *Ubc* mRNA in wild-type mice (see Fig. S3A and S3B in the supplemental material). Moreover, GFP expression in tissues from $Ubb^{+/-}$ and $Ubc^{+/-}$ mice, measured by indirect competitive ELISA, also correlated with expression of the corresponding genes assessed by measuring *Ubb* and *Ubc* mRNA levels in wild-type mice (see Fig. S3A and S3C in the supplemental material).

Comparison of *Ubb*- and *Ubc*- driven GFP-puro expression by direct visualization of GFP fluorescence in testes of 40-day-old mice heterozygous for the marked allele reveals that, although both genes are prominently expressed in Leydig cells, they exhibit minimally overlapping and largely complementary patterns of expression in seminiferous tubules (Fig. 6A). Although GFP expression in $Ubb^{+/-}$ testes is evident throughout the seminiferous epithelium including Sertoli cells, the band of fluorescence in a circumferential layer just above the basal layer of the epithelium, together with the absence of the classic

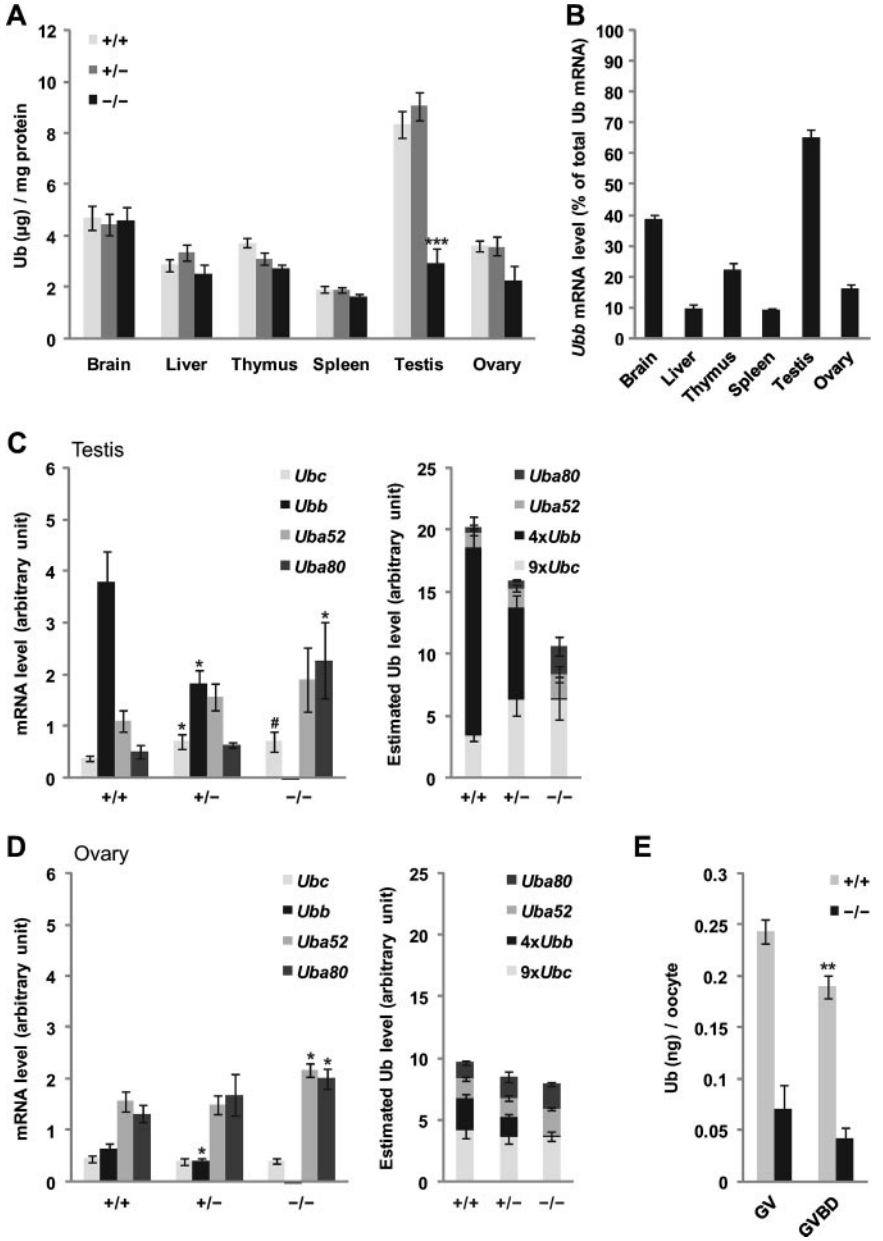


FIG. 5. Contribution of *Ubb* to maintenance of Ub levels. (A) Total Ub levels in various tissues. Tissues from 5-month-old $Ubb^{+/+}$, $Ubb^{+/-}$, and $Ubb^{-/-}$ were homogenized, and tissue lysates from brain, liver, thymus, spleen ($n = 5$ to 6 for +/+ and $n = 6$ for the other genotypes per tissue), testes (+/+, $n = 7$; +/−, $n = 4$; −/−, $n = 3$), and ovaries (+/+, $n = 4$; +/−, $n = 4$; −/−, $n = 3$) were treated with Usp2-cc (catalytic core of Ub-specific protease 2) and subjected to indirect competitive ELISA. Data are expressed as the mean ± standard error from the indicated number of mice from triplicate experiments for each sample. ***, $P < 0.001$ versus the same tissue of $Ubb^{+/+}$ mice. (B) *Ubb* mRNA levels in various tissues. Total RNA was isolated from various tissues in 5-month-old wild-type mice ($n = 7$ for testes, $n = 5$ for ovaries, and $n = 3$ for all other tissues). *Ubb*, *Ubc*, *Uba52*, and *Uba80* mRNA levels were measured by quantitative real-time RT-PCR. *Ubb* mRNA levels were expressed as percentages of total Ub (*Ubb*, *Ubc*, *Uba52*, and *Uba80*) mRNA levels in each tissue. Data are expressed as the mean ± standard error from the indicated number of mice. (C and D) (Left) Ub mRNA levels in testes (+/+, $n = 7$; +/−, $n = 4$; −/−, $n = 4$) and ovaries (+/+, $n = 5$; +/−, $n = 5$; −/−, $n = 6$) from 5-month-old mice. Total RNA was isolated from testes and ovaries, and *Ubc*, *Ubb*, *Uba52*, and *Uba80* mRNA levels were measured by quantitative real-time RT-PCR and normalized to β-actin levels. (Right) Relative contribution of Ub genes to total Ub levels in testes and ovaries. Contributions of four different Ub genes to total Ub levels are shown after normalization by the number of Ub moieties that each Ub transcript generates. Data are expressed as the mean ± standard error from the indicated number of mice. *, $P < 0.05$ versus corresponding Ub mRNA level in $Ubb^{+/+}$ mice. #, $P < 0.06$ versus *Ubc* mRNA level in $Ubb^{+/+}$ mice. (E) Total Ub levels in wild-type ($Ubb^{+/+}$) and $Ubb^{-/-}$ oocytes at different stages. Four-week-old females (+/+, $n = 10$; −/−, $n = 5$) were primed with PMSG and sacrificed 44 h later to collect oocytes. GV (+/+, $n = 338$; −/−, $n = 76$) and GVBD (+/+, $n = 359$; −/−, $n = 35$) oocytes were collected in two separate experiments and resuspended in 3 μl hypotonic buffer containing 0.1% digitonin. In each experiment, oocyte lysates were treated with Usp2-cc, divided into one to three aliquots for each stage, and subjected to indirect competitive ELISA. The average protein concentration in a wild-type oocyte is about 25 ng; therefore, the Ub content in a wild-type oocyte is about 1% of total protein. Data are expressed as the mean ± standard error from the total number of aliquots for each sample. **, $P < 0.01$ versus GV stage of $Ubb^{+/+}$ mice.

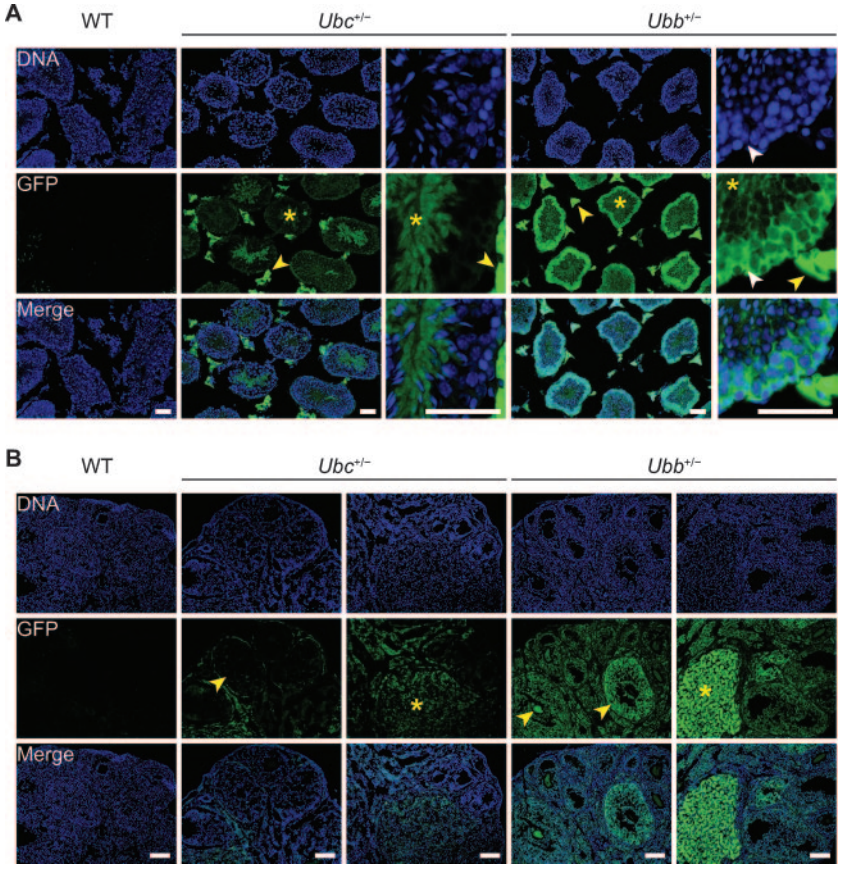


FIG. 6. Differential expression of *Ubb* and *Ubc* genes in testes and ovaries. (A) Frozen testicular sections were prepared from wild-type (WT), $Ubc^{+/-}$, and $Ubb^{+/-}$ mice at 40 days of age, and expression of *Ubb* and *Ubc* genes were monitored by direct GFP fluorescence using confocal microscopy. Both genes are highly expressed in Leydig cells (yellow arrowhead), while the expression pattern is different in seminiferous tubules (asterisk). In addition to spermatocytes, *Ubb* is also expressed in Sertoli cells (white arrowhead). Scale bar, 50 μm. (B) Frozen ovarian sections were prepared from wild-type (WT), $Ubc^{+/-}$, and $Ubb^{+/-}$ mice at 65 days of age, and expression of *Ubb* and *Ubc* genes was monitored by direct GFP fluorescence using confocal microscopy. *Ubb*, but not *Ubc*, is highly expressed in oocytes and granulosa cells (yellow arrowhead), while both genes are expressed in luteal cells (asterisk). Scale bar, 100 μm.

"spokes on a wheel" pattern, typical of Sertoli cells, is most consistent with predominant pattern of expression in spermatocytes. In sharp contrast, GFP expression in $Ubc^{+/-}$ testes is restricted to Leydig cells and elongating spermatids. GFP fluorescence in $Ubb^{-/-}$ testes is prominent in spermatogonia and arrested pachytene spermatocytes, as well as in Leydig cells (data not shown). These differences in GFP expression patterns within the seminiferous epithelium of $Ubb^{+/-}$ and $Ubc^{+/-}$ testes point to differences in endogenous promoter activity and reflect the preferential expression of the *Ubb* gene in developing germ cells.

In ovaries, the predominant role of *Ubb* over *Ubc* is most striking in oocytes and granulosa cells, as demonstrated by direct visualization of GFP fluorescence (Fig. 6B); GFP fluorescence is strong in follicles of $Ubb^{+/-}$ ovaries but much reduced in these cells in $Ubc^{+/-}$ ovaries. Interestingly, $Ubc^{+/-}$ ovaries exhibit strong GFP fluorescence in luteal cells, as in $Ubb^{+/-}$ ovaries. The high GFP expression in oocytes and granulosa cells from $Ubb^{+/-}$ ovaries, combined with the low expression of *Ubc* in these cells, strongly suggests that insufficient Ub in oocytes and their surrounding granulosa cells may be the principal cause of ovarian failure in $Ubb^{-/-}$ mice.

## DISCUSSION

Ub is an abundant protein that plays essential roles in multiple cellular processes in all eukaryotic cells. Yet disruption of *Ubb*, one of four ubiquitously expressed, seemingly redundant genes, leads to an arrest of meiotic progression in male and female germ cells, as well as degenerative changes to the testes. These findings suggest that *Ubb* plays roles in both meiotic progression and gonadal physiology. The similarity between the meiotic phenotypes in $Ubb^{-/-}$ germ cells and the sporulation defects observed in *ubi4* yeast signifies that this unique requirement for polyubiquitin gene expression in meiotic progression is remarkably conserved over more than a billion years of evolution.

The single polyubiquitin gene in budding (*UBI4*) or fission ($ubi4^{+}$; *Schizosaccharomyces pombe*) yeast is essential for meiosis and for survival under stress (12, 22). Our finding that $Ubc^{-/-}$ (29) but not $Ubb^{-/-}$ (data not shown) mouse embryonic fibroblasts exhibit increased stress sensitivity suggests that these dual functions of *UBI4*/$ubi4^{+}$ have been segregated into the two paralogous polyubiquitin genes in mammals. The finding that other organs in $Ubb^{-/-}$ mice develop normally sug-

gests that *Ubb* is not required for mitotic progression, consistent with the lack of growth or mitotic phenotypes in *ubi4* yeast (12, 22).

The $Ubb^{-/-}$ testes at 7 days of age are morphologically normal and do not exhibit greatly reduced numbers of germ cells. However, spermatocytes lacking *Ubb* are blocked in pachytene; they fail to enter the diplotene stage or progress to the first meiotic division phase to separate correctly synapsed chromosomes and eventually undergo cell death. This meiotic arrest suggests that the principal defect in $Ubb^{-/-}$ spermatogenesis occurs at or before the transition to the diplotene stage of prophase I. In contrast, the meiotic phenotype in female $Ubb^{-/-}$ mice is more heterogeneous, with some oocytes progressing to diplotene in vivo. The majority of oocytes isolated from $Ubb^{-/-}$ mice are competent to progress to GVBD, albeit more slowly, and a few are even able to form a metaphase spindle signifying the completion of prophase I. Like $Ubb^{-/-}$ oocytes, *ubi4* zygotes in fission yeast exhibit abnormal spindle morphology and impaired chromosome separation in meiosis I (22). The occasional *ubi4* zygotes observed to progress through the first meiotic division become arrested in the second (22). We propose that the heterogeneity in meiotic arrest in $Ubb^{-/-}$ oocytes and *ubi4* zygotes is the result of cell-to-cell variation in the amount of available Ub, underscoring the paramount and conserved role for polyubiquitin gene expression in meiotic progression. $ubi4^{+}$ transcription is highly induced during sporulation in fission yeast, yet cellular Ub levels do not appear to increase, leading to the surprising conclusion that Ub may be consumed during meiosis (22). (Ub is normally recycled by isopeptidases associated with the 26S proteasome.) Likewise, total Ub levels decrease between GV and GVBD in mouse oocytes in vitro (see Fig. 5E), suggesting that, as in yeast, significant amounts of Ub are consumed during meiotic progression. These parallels between mice and yeast support the conclusion that meiotic progression depends on expression of *Ubb*, most likely autonomously, in germ cells.

Although our data support the conclusion that *Ubb* constitutes the predominant source of Ub in germ cells, it is also clear that *Ubb* is expressed in somatic cells in the gonads, particularly those that, like Sertoli and granulosa cells, interact intimately with and support germ cells. Effects of *Ubb* loss are not limited to arrest of germ cell development during meiotic prophase; they include deficiencies in numbers of germ cells from early developmental stages as well as possible defects in supporting cells of the gonad (e.g., Sertoli cells display abnormal separation from the basement membrane) and ultimate atrophy of the gonads. The latter defect is not typical of other meiotic arrest or germ cell depletion phenotypes and thus cannot be explained solely by loss of meiotic germ cells. In testes, *Ubb* is expressed in somatic supporting cells, including Leydig cells and also Sertoli cells, and lack of Ub in these cells could account for detrimental gonadal degeneration phenotypes. Age-related gonadal atrophy may also be due to hypothalamic defects in the $Ubb^{-/-}$ mouse (K. Ryu et al., submitted for publication). Many, but not all, of the gonadal phenotypes exhibited by $Ubb^{-/-}$ mice are similar to phenotypes of mice with a deletion in the *Gnrh1* gene (the *hpg*, or hypogonadal, mouse) (17, 18). Male mice (and humans) with *Gnrh1* mutations exhibit small testes and arrest of spermatogenesis before the diplotene stage. However, female mice with *Gnrh1* mutations are much more severely impaired than $Ubb^{-/-}$ females and have only streak gonads at birth. These interesting possibilities could be tested experimentally by gonad and germ cell transplantation analyses and by the generation of cell-type-specific "conditional" *Ubb* knockouts to determine the cell autonomy of the various germ cell defects due to *Ubb* gene disruption.

Although the phenotype of the $Ubb^{-/-}$ ovaries may be complicated by the expression of *Ubb* in both the somatic and germ cell compartments, several scenarios may account for the markedly reduced size of the $Ubb^{-/-}$ ovaries. It is possible that $Ubb^{-/-}$ oogonia do not efficiently complete fetal meiotic prophase and a large number of them degenerate in a manner reminiscent of the pachytene demise observed during spermatogenesis. Thus, the pool of oocytes available to form follicles is probably already decreased at birth. However, the observation that follicle growth is also impaired may indicate that oocyte signals instructive for follicle formation and early growth are defective in $Ubb^{-/-}$ oocytes, causing inefficient folliculogenesis during postnatal life.

In spite of additional phenotypes with incomplete penetrance, $Ubb^{-/-}$ oocytes display a complete blockade of meiosis I progression and are unable to extrude a polar body. This is true even for the rare oocytes with an apparently normal spindle. This failure to progress to anaphase is most likely with the result of impaired function of APC/C (anaphase-promoting complex/cyclosome). As in mitosis, progression through the two meiotic divisions requires APC/C-mediated destruction of securin and cyclins (21, 30), underscoring an essential role for APC/C-mediated Ub conjugation in meiotic progression. How APC/C activity contributes to the separation of homologous chromosomes in meiosis I and the identity of meiosis-specific APC/C substrates remain unknown. Our data demonstrate that *Ubb* plays an essential role in maintaining the Ub supplies required for APC/C function and predict that undegraded meiosis-specific APC/C substrates should accumulate in $Ubb^{-/-}$ germ cells.

Although Ub is universally required for nearly all cellular processes, our data suggest that loss of *Ubb* gives rise to profound defects in germ cell maturation that are surprising in view of the fact that mitotic cell cycle is not obviously affected. Given the established roles of Ub-dependent proteolysis in regulating progression through the meiotic and mitotic cell cycles and given that the single polyubiquitin gene in yeast is also essential for meiosis and its absence cannot be compensated for by any of the other yeast ubiquitin genes, it is perhaps not surprising that a Ub gene knockout results in meiotic arrest. Therefore, the genes which encode Ub serve nonredundant functions and suggest the possibility of unanticipated meiotic roles that are conserved throughout eukaryotic evolution.

## ACKNOWLEDGMENTS

We thank our colleagues in the Kopito lab for helpful discussions and comments, and we are especially grateful to Catherine Gilchrist for help in screening the mouse genomic DNA library and Gregory Barsh for helpful discussion. We also thank the Transgenic Research Center for DNA microinjection, embryonic stem cell manipulation, and generation of chimeric mice.

This work was funded in part by a grant from the National Institute of Aging (to R.R.K.) and by grants from the National Institute of Child Health and Human Development (to M.A.H. and M.C.).

## REFERENCES


1. **Baarends, W. M., E. Wassenaar, R. van der Laan, J. Hoogerbrugge, E. Sleddens-Linkels, J. H. J. Hoeijmakers, P. de Boer, and J. A. Grootegoed.** 2005. Silencing of unpaired chromatin and histone H2A ubiquitination in mammalian meiosis. Mol. Cell. Biol. **25:**1041–1053.
2. **Baker, R. T., and P. G. Board.** 1991. The human ubiquitin-52 amino acid fusion protein gene shares several structural features with mammalian ribosomal protein genes. Nucleic Acids Res. **19:**1035–1040.
3. **Baker, R. T., and P. G. Board.** 1987. The human ubiquitin gene family: structure of a gene and pseudogenes from the Ub B subfamily. Nucleic Acids Res. **15:**443–463.
4. **Baker, R. T., A. M. Catanzariti, Y. Karunasekara, T. A. Soboleva, R. Sharwood, S. Whitney, and P. G. Board.** 2005. Using deubiquitylating enzymes as research tools. Methods Enzymol. **398:**540–554.
5. **Bas, A., G. Forsberg, S. Hammarstrom, and M. L. Hammarstrom.** 2004. Utility of the housekeeping genes 18S rRNA, beta-actin and glyceraldehyde-3-phosphate-dehydrogenase for normalization in real-time quantitative reverse transcriptase-polymerase chain reaction analysis of gene expression in human T lymphocytes. Scand. J. Immunol. **59:**566–573.
6. **Bond, U., and M. J. Schlesinger.** 1986. The chicken ubiquitin gene contains a heat shock promoter and expresses an unstable mRNA in heat-shocked cells. Mol. Cell. Biol. **6:**4602–4610.
7. **Borum, K.** 1961. Oogenesis in the mouse. A study of the meiotic prophase. Exp. Cell Res. **24:**495–507.
8. **Catanzariti, A. M., T. A. Soboleva, D. A. Jans, P. G. Board, and R. T. Baker.** 2004. An efficient system for high-level expression and easy purification of authentic recombinant proteins. Protein Sci. **13:**1331–1339.
9. **D'Andrea, A., and D. Pellman.** 1998. Deubiquitinating enzymes: a new class of biological regulators. Crit. Rev. Biochem. Mol. Biol. **33:**337–352.
10. **Enders, G. C., and J. J. May II.** 1994. Developmentally regulated expression of a mouse germ cell nuclear antigen examined from embryonic day 11 to adult in male and female mice. Dev. Biol. **163:**331–340.
11. **Finley, D., B. Bartel, and A. Varshavsky.** 1989. The tails of ubiquitin precursors are ribosomal proteins whose fusion to ubiquitin facilitates ribosome biogenesis. Nature **338:**394–401.
12. **Finley, D., E. Ozkaynak, and A. Varshavsky.** 1987. The yeast polyubiquitin gene is essential for resistance to high temperatures, starvation, and other stresses. Cell **48:**1035–1046.
13. **Fornace, A. J., Jr., I. Alamo, Jr., M. C. Hollander, and E. Lamoreaux.** 1989. Ubiquitin mRNA is a major stress-induced transcript in mammalian cells. Nucleic Acids Res. **17:**1215–1230.
14. **Hershko, A., and A. Ciechanover.** 1998. The ubiquitin system. Annu. Rev. Biochem. **67:**425–479.
15. **Hochstrasser, M.** 1996. Ubiquitin-dependent protein degradation. Annu. Rev. Genet. **30:**405–439.
16. **Lund, P. K., B. M. Moats-Staats, J. G. Simmons, E. Hoyt, A. J. D'Ercole, F. Martin, and J. J. Van Wyk.** 1985. Nucleotide sequence analysis of a cDNA encoding human ubiquitin reveals that ubiquitin is synthesized as a precursor. J. Biol. Chem. **260:**7609–7613.
17. **Mason, A. J., J. S. Hayflick, R. T. Zoeller, W. S. Young III, H. S. Phillips, K. Nikolics, and P. H. Seeburg.** 1986. A deletion truncating the gonadotropin-releasing hormone gene is responsible for hypogonadism in the hpg mouse. Science **234:**1366–1371.
18. **Mason, A. J., S. L. Pitts, K. Nikolics, E. Szonyi, J. N. Wilcox, P. H. Seeburg, and T. A. Stewart.** 1986. The hypogonadal mouse: reproductive functions restored by gene therapy. Science **234:**1372–1378.
19. **Mehlmann, L. M., T. L. Jones, and L. A. Jaffe.** 2002. Meiotic arrest in the mouse follicle maintained by a Gs protein in the oocyte. Science **297:**1343–1345.
20. **Meistrich, M. L., W. R. Bruce, and Y. Clermont.** 1973. Cellular composition of fractions of mouse testis cells following velocity sedimentation separation. Exp. Cell Res. **79:**213–227.
21. **Oelschlaegel, T., M. Schwickart, J. Matos, A. Bogdanova, A. Camasses, J. Havlis, A. Shevchenko, and W. Zachariae.** 2005. The yeast APC/C subunit Mnd2 prevents premature sister chromatid separation triggered by the meiosis-specific APC/C-Ama1. Cell **120:**773–788.
22. **Okazaki, K., H. Okayama, and O. Niwa.** 2000. The polyubiquitin gene is essential for meiosis in fission yeast. Exp. Cell Res. **254:**143–152.
23. **Ozkaynak, E., D. Finley, and A. Varshavsky.** 1984. The yeast ubiquitin gene: head-to-tail repeats encoding a polyubiquitin precursor protein. Nature **312:**663–666.
24. **Peters, H.** 1969. The development of the mouse ovary from birth to maturity. Acta Endocrinol. (Copenhagen) **62:**98–116.
25. **Redman, K. L., and M. Rechsteiner.** 1989. Identification of the long ubiquitin extension as ribosomal protein S27a. Nature **338:**438–440.
26. **Reed, S. I.** 2003. Ratchets and clocks: the cell cycle, ubiquitylation and protein turnover. Nat. Rev. Mol. Cell Biol. **4:**855–864.
27. **Reinholdt, L., T. Ashley, J. Schimenti, and N. Shima.** 2004. Forward genetic screens for meiotic and mitotic recombination-defective mutants in mice. Methods Mol. Biol. **262:**87–107.
28. **Ryu, K. Y., R. T. Baker, and R. R. Kopito.** 2006. Ubiquitin-specific protease 2 as a tool for quantification of total ubiquitin levels in biological specimens. Anal. Biochem. **353:**153–155.
29. **Ryu, K. Y., R. Maehr, C. A. Gilchrist, M. A. Long, D. M. Bouley, B. Mueller, H. L. Ploegh, and R. R. Kopito.** 2007. The mouse polyubiquitin gene UbC is essential for fetal liver development, cell-cycle progression and stress tolerance. EMBO J. **26:**2693–2706.
30. **Salah, S. M., and K. Nasmyth.** 2000. Destruction of the securin Pds1p occurs at the onset of anaphase during both meiotic divisions in yeast. Chromosoma **109:**27–34.
31. **Sorensen, R. A., and P. M. Wassarman.** 1976. Relationship between growth and meiotic maturation of the mouse oocyte. Dev. Biol. **50:**531–536.
32. **Wiborg, O., M. S. Pedersen, A. Wind, L. E. Berglund, K. A. Marcker, and J. Vuust.** 1985. The human ubiquitin multigene family: some genes contain multiple directly repeated ubiquitin coding sequences. EMBO J. **4:**755–759.